

Solute-mediated interactions between active droplets

Pepijn G. Moerman,^{1,2} Henrique W. Moyses,¹ Ernest B. van der Wee,² David G. Grier,¹ Alfons van Blaaderen,² Willem K. Kegel,² Jan Groenewold,^{2,3} and Jasna Brujic^{1,*}

¹*Center for Soft Matter Research, Department of Physics, New York University, New York, New York 10003, USA*

²*Debye Institute for Nanomaterials Science, Utrecht University, 3584 Utrecht, The Netherlands*

³*Academy of Advanced Optoelectronics, South China Normal University, Guangzhou, China*

(Received 25 February 2017; revised manuscript received 15 May 2017; published 15 September 2017)

Concentration gradients play a critical role in embryogenesis, bacterial locomotion, as well as the motility of active particles. Particles develop concentration profiles around them by dissolution, adsorption, or the reactivity of surface species. These gradients change the surface energy of the particles, driving both their self-propulsion and governing their interactions. Here, we uncover a regime in which solute gradients mediate interactions between slowly dissolving droplets without causing autophoresis. This decoupling allows us to directly measure the steady-state, repulsive force, which scales with interparticle distance as $F \sim 1/r^2$. Our results show that the dissolution process is diffusion rather than reaction rate limited, and the theoretical model captures the dependence of the interactions on droplet size and solute concentration, using a single fit parameter, $l = 16 \pm 3$ nm, which corresponds to the length scale of a swollen micelle. Our results shed light on the out-of-equilibrium behavior of particles with surface reactivity.

DOI: [10.1103/PhysRevE.96.032607](https://doi.org/10.1103/PhysRevE.96.032607)

I. INTRODUCTION

Active particles build up concentration gradients in their surroundings and locally alter the composition of their solvent. This process can occur if the particles dissolve, or if they adsorb other species from the solution, or if their surfaces catalyze chemical reactions. Examples include heterogeneous catalysts [1,2], droplets undergoing Ostwald ripening, silica particles dissolving in a strong base, ion-exchange resin particles [3], and microbes that are consuming nutrients or excreting signaling proteins [4,5]. These concentration profiles can affect the behavior of the dispersed particles if their surface tension couples to the solute concentration [2,6–9]. The most studied example is given by autophoretic swimmers, whose asymmetric concentration profiles cause the particles to swim [10–13]. As a result, they move in a directional manner, giving rise to dynamic patterns [1,14–16]. These particles constitute a model system for studying out-of-equilibrium pattern formation [17] and dynamic clustering [14,16,18]. Nevertheless, the propulsion mechanism of many of these model systems is not well understood [19], and their mutual interactions even less so.

In the case of particles that are self-propelled by chemical gradients, the overlap of concentration profiles around two or more particles results in mutual interactions [2,7,20,21]. These interactions are coupled to the self-propulsion mechanism and have therefore not been measured independently. Here, we uncover a regime in which active droplets do not swim, but do exude concentration profiles. This system allows us to measure the gradient-mediated interactions between pairs of droplets in the absence of autophoresis. We then develop a theoretical model based on steady-state diffusion profiles for the functional form of the droplet-droplet interaction. This model allows us to fit the data as a function of droplet size and solute concentration to elucidate the underlying microscopic process. This “static” case improves our understanding of the threshold concentration above which the droplets begin to swim.

II. EXPERIMENTAL SYSTEM

We employ a simple model system of droplets of di-ethyl phthalate (DEP) oil dispersed in an aqueous solution of the surfactant sodium dodecyl sulphate (SDS). The DEP droplets slowly dissolve in the medium, giving rise to local concentration gradients. DEP is only marginally soluble in water (0.2 mg/ml). Above a threshold SDS concentration of 4 mM, surfactant molecules and DEP molecules from the droplet co-assemble to form oily micelles, causing the droplets to shrink at a rate that depends on the SDS concentration. This process, schematically depicted in Fig. 1(a), depletes the surfactant molecules near the surface and results in a radially symmetric concentration profile of SDS. Figure 1(b) shows that the surface tension between water and DEP decreases with SDS monomer concentration, measured using the pendant drop method [22]. This coupling between the surface free energy of the particle and the surfactant monomer content causes droplets to move towards higher SDS concentrations in the bulk, due to the Marangoni effect [23,24].

Initially, the dissolution leads to an isotropic concentration profile and no net force acts on the particle. Above a given dissolution rate, however, the isotropic state becomes unstable and any fluctuation (mechanical or thermal) gives rise to self-sustained motion in a random direction [25–27]. The self-propelled droplets repel one another, as shown in the examples shown in Fig. 1(c) and in Ref. [28]. To measure the effective interparticle repulsion due to the overlap of their solute profiles, here we focus on the regime of SDS concentrations in which the droplets are surrounded by a symmetric concentration profile and do not swim. Experimentally, this regime exists between 4 mM SDS, below which the droplets are insoluble, and 8 mM SDS, above which the droplets swim.

III. SOLUTE-MEDIATED INTERACTIONS

In this regime, we measured the interaction strength between dissolving droplets using optical tweezers [29,30] (see Appendix A). Two holographically projected optical traps

*Corresponding author: jb2929@nyu.edu

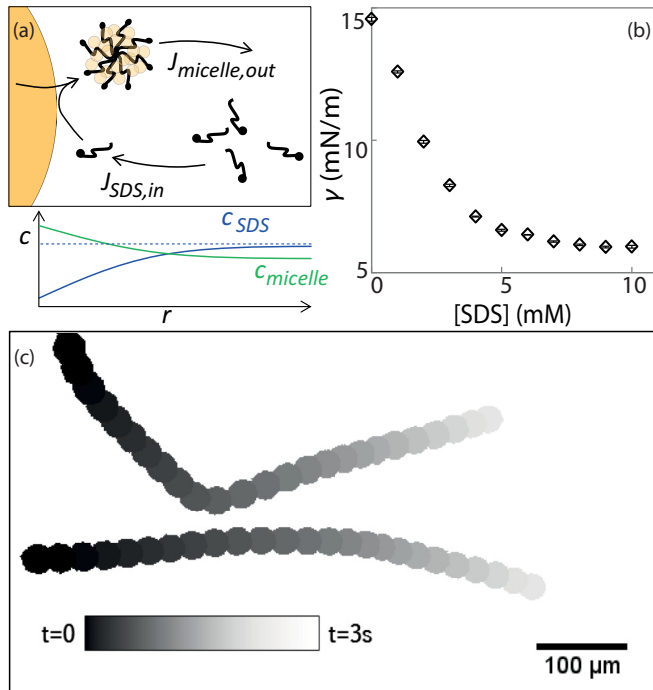


FIG. 1. Droplet interactions due to surfactant gradients. (a) Schematic overview of DEP droplet dissolution into swollen SDS micelles, giving rise to radial concentration gradients of SDS monomer (blue line) and micelles (green line) surrounding the droplet surface, compared to the bulk concentration (dashed line). (b) Surface tension of DEP droplets in water decreases as a function of the SDS concentration. (c) Two oil droplets swimming in given initial directions repel one another as a result of their concentration gradients. Circles map their trajectories over time.

were used to bring two droplets close together and then released to allow the particles to move under the influence of the interaction force. Figure 2(a) and Ref. [28] show a typical time sequence as the particles move apart during one such cycle. In Fig. 2(b), we give a schematic overview of the overlapping concentration profiles that induce an effective interaction. We obtain an estimate for the interaction force by analyzing images of the particle motion. The time trace of the center-to-center separation, $r(t)$, is plotted in Fig. 2(c). The derivative of this trajectory yields the relative separation speed, $U(r)$, examples of which are plotted in Fig. 2(d) as a function of droplet size. The droplets range in diameter from 15 to 45 μm , and therefore exhibit no Brownian motion. They move with maximum speeds below 40 $\mu m/s$, and thus still have a low Reynolds number. Their relative speed is therefore directly proportional to their effective interaction force.

The larger the droplets, the stronger the repulsive interaction, as shown by the data in Fig. 2(d). In all cases, the range of the interaction exceeds 50 μm , which is much longer than that expected for electrostatic interactions. The Debye-Huckel screening length is less than 10 nm at the ionic strengths of our experiments. The fact that experiments performed at SDS concentrations below 5 mM show no repulsion confirms that the repulsion is concomitant with the formation of DEP-swollen micelles of SDS. As the SDS concentration is increased, the

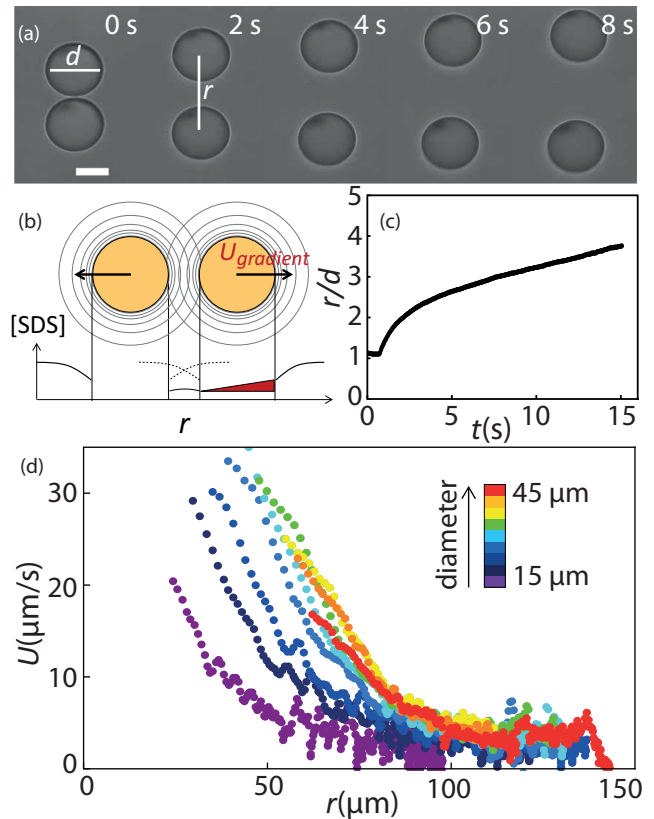


FIG. 2. Solvent-induced droplet interactions. (a) Frames of a movie showing two oil droplets moving away from each other due to the solute-mediated repulsion after they have been brought into contact using optical tweezers. (b) Schematic drawing shows how overlapping SDS concentration profiles lead to droplet interactions. The red triangle represents the gradient causing the motion. (c) Measurements of interdroplet separation as a function of time allow us to determine their size-dependent velocity U as a function of separation in (d).

DEP dissolves faster into the micelles, creating a steeper gradient, which results in an increased interaction strength.

IV. HOVERING DROPLETS

The velocity caused by solute gradients is of the same order of magnitude as the sedimentation velocity under gravity. This allows for an alternative measurement of the strength of a solute-mediated interaction by balancing it with gravity (see Appendix A). The top panel of Fig. 3(a) shows images of dissolving droplets through a tilted microscope. The top feature is an image of the actual droplet and the bottom feature is an optical reflection in the glass slide. The droplet height is then half the distance between the droplet and its mirror image. Figure 3(a) shows that particles with a diameter over 30 μm make contact with the glass slide because their sedimentation velocity is larger than the solute-mediated interaction velocity. For smaller particles, however, the two speeds are comparable, resulting in an equilibrium hovering height above the glass cover slide at which the two oppositely directed velocities cancel out.

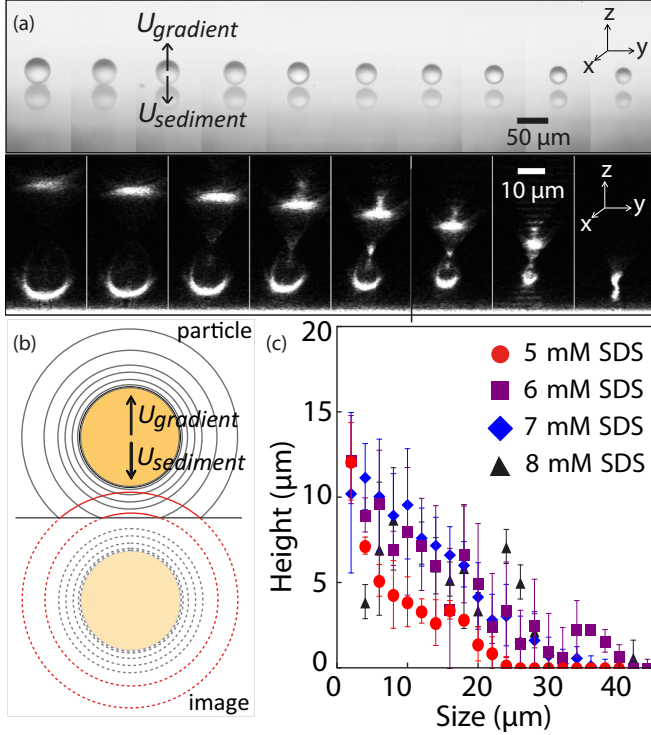


FIG. 3. Hovering due to solute-mediated interactions. (a) Top panel shows a dissolving DEP droplet through a tilted bright-field microscope. The top feature is the real droplet and the lower feature the optical image on the glass slide. Bottom panel shows xz projections of the same droplets imaged in reflection mode on a confocal microscope. (b) Schematic drawing shows how a solute cloud around a particle can lift it from the glass surface against gravity. (c) Measured droplet hovering heights are plotted as a function of their size. Error bars come from repeated measurements.

The lower panel in Fig. 3(a) shows the same set of experiments performed using confocal microscopy in reflection mode. The elongated shape of the image is caused by internal reflection inside the droplet and the correct measure of the droplet size is the width of the bottom half-sphere. The schematic drawing in Fig. 3(b) explains how the solute-mediated interaction that causes repulsion between two droplets is also responsible for the hovering of a single droplet above a glass surface. The SDS concentration around the droplet is lower near the glass slide, because no influx of SDS molecules is possible through the glass. This exclusion of SDS monomers also occurs between two dissolving droplets, as shown in Fig. 2(b), resulting in similar solute-mediated interaction speeds. Figure 3(c) shows the equilibrium height of droplets of various SDS concentrations and sizes, highlighting the trend that smaller droplets at higher SDS concentrations hover at higher altitude.

V. MODELING MOTION IN A SOLUTE GRADIENT

Next, we present a theoretical model for the functional form of the interaction strength between two droplets. The speed of a droplet in the concentration profile of its neighbor

$$U = M \nabla c_s, \quad (1)$$

where ∇c_s is the concentration gradient along the surface and M is the particle mobility. For a droplet, the mobility is given by [9,23–25]

$$M = \frac{2aK}{3(2\eta_o + 3\eta_i)}, \quad (2)$$

where a is the droplet radius, K is the slope of the surface tension versus the SDS concentration graph in Fig. 1(b), and η_o and η_i are the viscosities of the continuous and dispersed phases, respectively. The gradient in which the droplet moves depends on the SDS concentration profile c_e generated by its neighbor.

To find ∇c_e , we consider the dissolution process of a single DEP droplet in an aqueous SDS solution. We assume that all oil transport from the droplet into the aqueous phase is mediated by SDS and that a steady-state diffusion profile develops after an initial transient state. This steady-state approximation is valid when particle motion is much slower than solute motion. The shape of the spherically symmetric concentration profile $c_e = C_1 + C_2/r$ then follows directly from Fick's law. Here, C_1 and C_2 are integration constants and r is the distance to the droplet center. Imposing the general boundary condition that the diffusive SDS flux to the surface $j_{\text{diff}} = -D \frac{dc}{dr} |_{r=a}$ must equal the rate at which SDS is consumed to form swollen micelles $j_{\text{react}} = k(c(a) - c^*)$ (see Appendix B), we obtain expressions for the integration constants and find that the slope of the profile generated by the neighboring droplet is given by

$$\nabla c_e = \frac{(c_\infty - c^*) a}{1 + l/a} \frac{1}{r^2}, \quad (3)$$

where c_∞ is the bulk SDS concentration and c^* is a threshold concentration, which is similar to the critical micelle concentration, but applies to DEP-swollen micelles of SDS. For these micelles, we measured that $c^* = 4$ mM. The quantity $l = D/k$ is a length obtained by dividing the diffusion coefficient D by the dissolution speed k , i.e., the speed at which oil moves across the droplet surface. This length scale l is indicative of whether the dissolution rate of DEP is diffusion or reaction limited. The theoretical limit $l/a \ll 1$ corresponds to a constant surface SDS concentration, consistent with a diffusion-limited assembly of DEP swollen micelles. The opposite limit, $l/a \gg 1$, indicates a constant dissolution rate, which is indicative of a reaction-limited assembly process. Plotting the rate of the dissolution rate $A = da/dt$ as a function of particle size a , as shown in Fig. 4, reveals a scaling with the droplet curvature $1/a$. This result lends support to a diffusion-limited mechanism for the dissolution of DEP into swollen micelles of SDS.

To first order, the speed U of the interacting droplets in Fig. 2 follows the $1/r^2$ scaling in Eq. (3). In addition, the external gradient ∇c_e imposed by the neighboring droplet is modified by two effects. First, the moving droplet is also dissolving, locally removing SDS from the external profile, as shown in Fig. 5(a). Second, advection around the moving droplet transports solute from the front to the back of the particle. These effects need to be quantified to capture the dependence of the interaction strength on droplet size and SDS concentration.

VI. DISSOLUTION IN AN EXTERNAL GRADIENT

To obtain the modification of ∇c_s due to the dissolution of the moving droplet, we consider a particle dissolving in the presence of a linear external gradient G_{ext} . Solving the diffusion equation then gives the steady-state concentration profile (see Appendix C)

$$c(r, \theta) = c_\infty - \frac{(c_\infty - c^*)}{1 + l/a} \frac{1}{r} + G_{\text{ext}} \cos(\theta) \left(r - a^3 \frac{1 - l/a}{1 + 2l/a} \frac{1}{r^2} \right). \quad (4)$$

Taking the derivative of Eq. (4) with respect to the radial distance r gives the relation between the gradient along the surface ∇c_s and the external gradient G_{ext} :

$$\nabla c_s = \frac{3l/a}{1 + 2l/a} G_{\text{ext}} \approx \frac{3l}{a} \nabla c_e. \quad (5)$$

In the second step of Eq. (5), we assume that the external gradient due to the dissolution of a neighboring droplet ∇c_e is approximately linear along the droplet surface since the process is diffusion limited ($l/a \ll 1$). In our case, the surface gradient is diminished, as shown in Fig. 5(b). On the other hand, in the reaction-limited case ($l/a \gg 1$) the surface gradient is enhanced compared to the external gradient, as shown in Fig. 5(c). It is therefore important to distinguish between the two microscopic mechanisms.

VII. AUTOPHORETIC ENHANCEMENT AND SELF-PROPULSION

The other modification to the external gradient arises due to the same effect that drives self-propulsion of a single particle. As an active particle moves, advection causes accumulation of the solute at the back of the particle, resulting in a self-induced concentration difference between the front and the back of the droplet Δc_e . This concentration difference over the particle

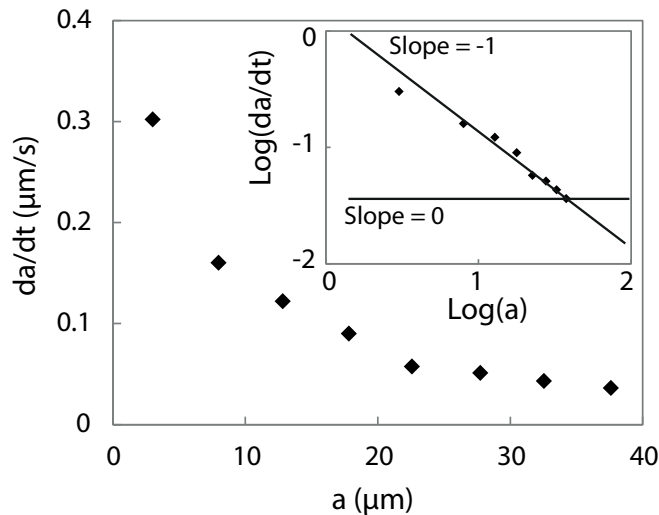


FIG. 4. Dissolution rate of a DEP droplet in a bath of 5 mM SDS as a function of particle size. Inset shows the log-log representation and reveals a slope of -1 , consistent with a diffusion-limited dissolution.

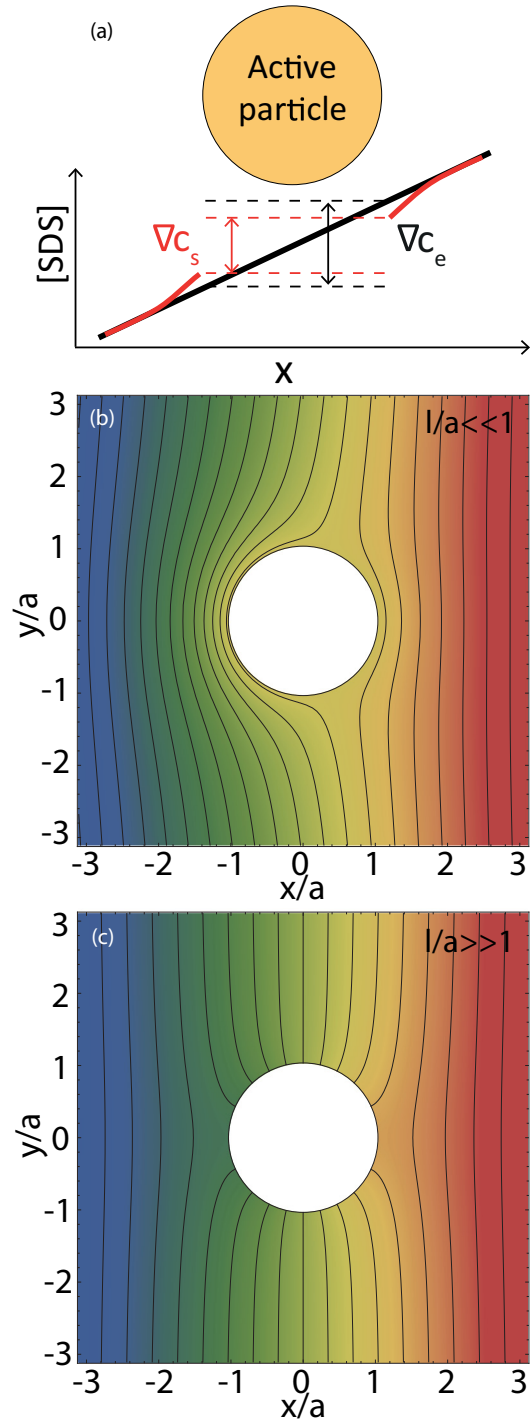


FIG. 5. (a) Schematic drawing of the effect of surface activity on an external gradient. The solid black line represents an unperturbed external gradient in which the active particle is positioned. Due to the activity of the particle the concentration profile is modified as shown by the solid red line. The difference in concentration between the back and the front of the droplet, indicated by the dashed black and red lines, is modified due to the dissolution of the active particle. (b) and (c) show the solute concentration profiles for a diffusion-limited and a reaction-limited dissolution, respectively, in an external gradient. These profiles are calculated with Eq. (4) with $G_{\text{ext}} = 1$, $c^* = 1$, $a = 1$, $c_\infty = 0$, $l/a = 10^{-3}$ in (b) and $l/a = 10^3$ in (c). Color map indicates increasing SDS concentration from blue to red. The black lines are isoconcentration lines.

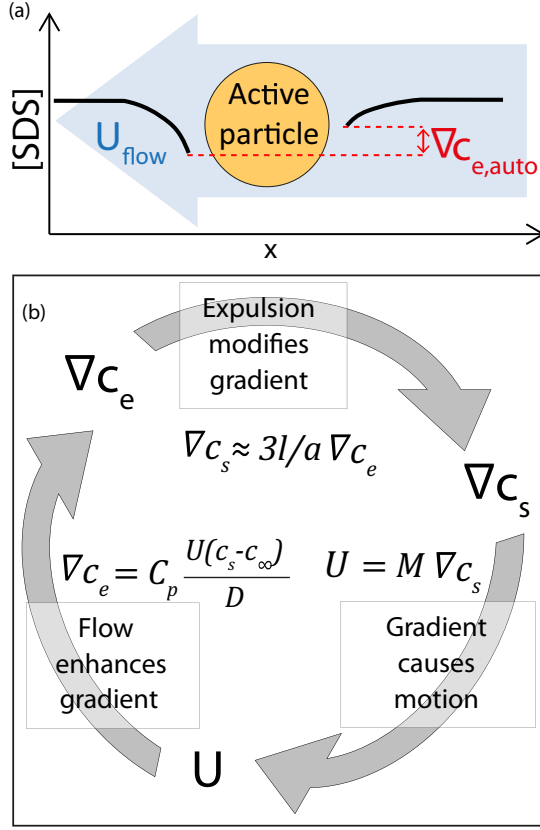


FIG. 6. Coupling between the advective flow and the solute gradient leads to self-propulsion. (a) Schematic drawing of the flow around a moving particle, which transports solute from the front to the back, resulting in an external gradient. (b) The autophoresis loop depicts the coupling between the solute profile and the flow from panel (a), which can lead to self-sustained motion.

diameter can be seen as an average gradient $\nabla c_{e,\text{auto}}$ that drives the particle motion. This process is schematically depicted in Fig. 6. In the limit of low particle speed U , the advective flux j_{adv} is linear with the flow velocity so that $j_{\text{adv}} = C_p U(c_s - c_\infty)$, where C_p is a dimensionless proportionality constant. The buildup of an external gradient due to advection is counteracted by a diffusive flux $j_{\text{diff}} = D \nabla c_e$. In steady state, these fluxes balance to give a motion-induced gradient $\nabla c_{e,\text{auto}}$ for a given droplet speed U :

$$\nabla c_{e,\text{auto}} = C_p \frac{U(c_s - c_\infty)}{D}. \quad (6)$$

Next, we deduce the criterion for self-propulsion in the absence of an external gradient where the gradient driving the motion is only the self-induced gradient, i.e., $\nabla c_e = \nabla c_{e,\text{auto}}$. The gradient along the droplet surface ∇c_s depends on ∇c_e , as shown in (5). Therefore, from (1) we find the requirement for self-sustained droplet motion with speed U^* as

$$U^* = M \frac{\nabla c_s}{\nabla c_e} C_p \frac{U^*(c_s - c_\infty)}{D}. \quad (7)$$

We find that either $U^* = 0$ in the static case or at $M \frac{\nabla c_s}{\nabla c_e} C_p \frac{(c_s - c_\infty)}{D} = 1$, U^* is a constant that corresponds to self-propulsion. We can write this requirement for self-propulsion in terms of the Peclet number, as defined by Michelin *et al.*

[26]. Using the definition of the SDS dissolution rate $A = -D \frac{dc}{dr}|_{r=a}$, we obtain $M \frac{\nabla c_s}{\nabla c_e} \frac{Aa}{D} = 1/C_p$. The left-hand side of this equation is similar to the Peclet number, such that the critical Peclet number for autophoresis in the absence of an external gradient is $\text{Pe}_{\text{cr}} = 1/C_p$.

Even below this self-propulsion threshold, the speed at which two particles move away from each other is enhanced by the coupling between the advective flow and the solute gradient. The total gradient around a particle is then the sum of the externally imposed gradient ∇c_e and the self-induced gradient $\nabla c_{e,\text{auto}}(U)$, such that the droplet speed is given by

$$U = M \frac{\nabla c_s}{\nabla c_e} [\nabla c_e + \nabla c_{e,\text{auto}}(U)]. \quad (8)$$

Solving for U gives the self-sustained swimming speed of a droplet in the gradient of its neighbor in terms of the above-described Peclet number:

$$U(r) = M \frac{\nabla c_s}{\nabla c_e} \frac{1}{1 - \frac{\text{Pe}}{\text{Pe}_{\text{cr}}}} \nabla c_e. \quad (9)$$

Here, the term $\frac{1}{1 - \frac{\text{Pe}}{\text{Pe}_{\text{cr}}}}$ is the autophoretic enhancement correction. In the limit of $l/a \ll 1$ and given that the Peclet number $\text{Pe} \propto c_\infty - c^*$ and that $\text{Pe}_{\text{cr}} \propto c_{\text{cr}} - c^*$, we can rewrite Eq. (9) in terms of experimentally accessible parameters so that we can compare with the data presented in Figs. 2 and 3:

$$U(r) = \frac{2aK}{(2\eta_o + 3\eta_i)} \frac{(c_\infty - c^*) l (c_{\text{cr}} - c^*)}{(c_{\text{cr}} - c_\infty) r^2}. \quad (10)$$

Here, $c_{\text{cr}} = 9$ mM is the threshold SDS concentration where self-propulsion is observed to occur.

VIII. COMPARING MODEL AND EXPERIMENTS

Using Eq. (10), we rescale all the data shown in Fig. 7(a) onto the master curve in Fig. 7(b). The log-log plot reveals a consistency with the predicted power-law scaling with distance as $\propto 1/r^2$ (black line) and the collapse of the data indicates that the scaling of droplet speed with size a and SDS concentration c_∞ are well captured by Eq. (10).

Using the fact that $K = 0.11$ mN m^{-1} mM^{-1} from the fit to the high SDS concentration regime of Fig. 1(b), we find that $l = 16 \pm 3$ nm, in agreement with the earlier observation that $l/a \ll 1$ and that the dissolution process is diffusion limited. This length scale coincides with the size of an oily micelle, to within an order of magnitude. The obtained value for the fit parameter can be related to the critical Peclet number Pe_{cr} at which self-propulsion occurs. When $l/a \ll 1$, Pe_{cr} is found by evaluating equation (10) at the SDS concentration at which self-propulsion begins to occur:

$$\text{Pe} \approx \frac{2K(c_{\text{cr}} - c^*)l}{(2\eta_o + 3\eta_i)D}. \quad (11)$$

Using the diffusion coefficient of oily micelles $D = 10^{-10}$ m^2 s^{-1} [31], we find $\text{Pe}_{\text{cr}} = 5$, which is in good agreement with the theoretically predicted value of $\text{Pe}_{\text{cr}} = 4$ in Ref. [26]. This connection between the onset of autophoretic motion and solute-mediated interactions highlights that both are due to the same effect. It is therefore not expected that autophoretic swimmers without solute-mediated interactions

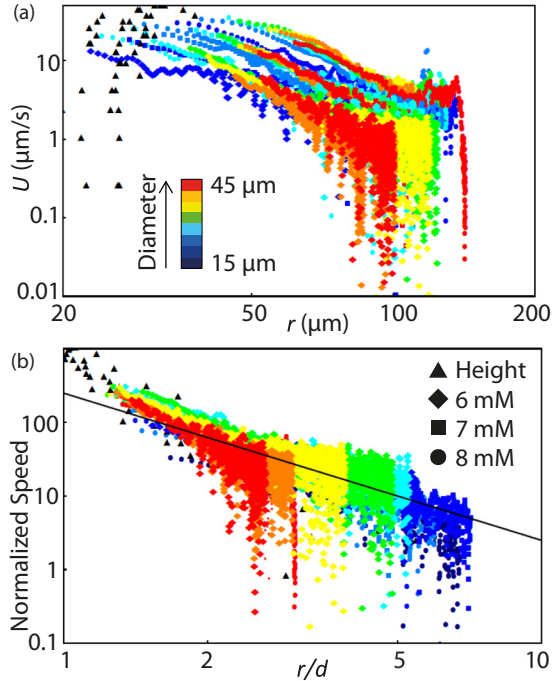


FIG. 7. Rescaling of active interactions. (a) Log-log representation of the speed with which droplets move away from each other as a function of interparticle distance. Color represents the initial droplet size and symbols represent SDS concentration. The data from the hovering experiment are indicated in black. (b) Data shown in (a), normalized using Eq. (10). The black line is a fit with a fixed slope of -2 .

exist, which has ramifications for the interpretation of activity-induced clustering and pattern formation.

IX. CONCLUSIONS

In conclusion, we developed an experimental model system of dissolving droplets to directly measure solute-mediated interactions. From a combination of tweezer experiments and balancing solute-mediated interactions with sedimentation, we measured the range of the interaction as well as the scaling with SDS concentration and droplet size. A simple theoretical model predicts these dependencies and connects the interaction strength with the self-propulsion threshold. This connection suggests that all reactive and dissolving particles, and in particular autophoretic swimmers, are subject to the same type of solute-mediated interactions. The interaction strength depends on the rate at which the reaction or dissolution process occurs and the sensitivity of the particles to the surrounding gradient. The functional form, given by Eq. (9), is general for isotropic particles in a steady state and is expected to be universally applicable.

ACKNOWLEDGMENTS

We thank Daan Frenkel, Eric Vanden-Eijnden, and Gerhard Blab for insightful discussions. This work was supported primarily by the Materials Research Science and Engineering Center (MRSEC) program of the National Science Foundation under Award No. DMR-1420073. J.B. acknowledges

support by the National Science Foundation under Grant No. DMR-1710163. E.W. and A.B. acknowledge financial support from the European Research Council under the European Union Seventh Framework Programme (Grant No. FP/2007-2013)/ERC Grant Agreement No. [291667] HierarSACo and from the NWO Graduate Program.

APPENDIX A: MATERIALS AND METHODS

1. Microfluidics

Droplets for optical tweezer experiments were prepared using a glass microfluidic device [32] with a round tapered inner capillary with inner diameter $30 \mu\text{m}$ in a square outer capillary with inner edge length $50 \mu\text{m}$. Capillaries were supplied by VitroCom. The inner capillary has a tip with a diameter of approximately $5 \mu\text{m}$. A 10 mM SDS (supplier: Sigma Aldrich) solution saturated with DEP (supplier: Sigma Aldrich) was flowed through a Merck Millipore hydrophilic PTFE membrane filter with pore size $0.45 \mu\text{m}$ and consecutively through the outer capillary. Pure DEP was pushed through a Merck Millipore hydrophobic PVDF membrane filter with pore size $0.45 \mu\text{m}$ and consecutively through the inner capillary using a pressure of 10 psi , using a pressure gauge. Nitrogen was used as the pressurizing gas. Droplet size was adjusted by varying pressure of the external flow: approximately 20 psi for $30 \mu\text{m}$ droplets. Size was determined by imaging the droplets using an Olympus microscope equipped with a Thorlabs camera. Droplets were collected in a glass container and stored no more than one week. Droplets for height measurements were prepared by shaking a mixture of $50 \mu\text{l}$ DEP and 1 ml of a DEP-saturated 10 mM SDS solution.

2. Dynamic measurements with optical tweezers

Two microliters of emulsion obtained from the microfluidic device was dispersed in a $500 \mu\text{l}$ bath of SDS solution of various SDS concentrations. Using a home-built optical tweezer setup [30], containing an IPG Photonics YLR-10 laser emitting at 1064 nm and a HoloEye PLUTO special light modulator, two droplets were collected from the cluster in the center of the sample, pushed next to each other, and dragged to an environment with no droplets in an area with a diameter of at least 10 droplet diameters. There the droplets were released and the motion was recorded using a home-built bright-field microscopy setup, containing a NECTI 324AII camera and a Nikon $100\times$ oil immersion objective ($\text{NA} = 1.45$). After a time interval of approximately 30 seconds, the droplets were pushed together and moved to a new clean environment and released again. Since the droplets shrink over time, this yielded data for various droplet sizes.

3. Solute force measurements under gravity

Two microliters of emulsion obtained from mechanical agitation was dispersed in a 1 ml bath of SDS solution of various SDS concentrations. For the tilted bright field microscopy images, the sample container was a home-built container from Menzel-Gläser No. 1 glass slides with a small piece of mirror on the bottom. Droplets of various sizes were imaged in the vicinity of no other droplets. A similar

sample was put on an inverted Leica SP8 confocal microscope equipped with a 40 \times /1.25 Leica confocal oil immersion objective, where the z stacks were recorded in reflection mode (wavelength $\lambda = 488$ nm). To correct for elongation in the z dimension due to the refractive index mismatch between glass and water the method by Besseling *et al.* [33] was used. Using a Menzel-Gläser No. 1.5 coverslip for imaging an aqueous sample with $n_D^{25} = 1.33$ while using a 40 \times /1.25 immersion oil objective with $n_D^{25} = 1.52$, we found and used a correction factor for the z scaling of 0.846.

4. Surface tension measurements

The densities of pure DEP and DEP-saturated SDS solutions of various concentrations were determined using a DMA 4500M Anton Paar density meter. The shape of DEP droplets in solutions with various SDS concentrations was measured using an Attension pendant drop tensiometer equipped with a DMK 21AU04 Imaging Source camera. From this the surface tension between DEP and water with various SDS concentrations was calculated.

5. Solubility measurements

DEP-saturated SDS solutions of various SDS concentrations were prepared by adding 2 ml of DEP to 10 ml aqueous SDS solutions and shaking vigorously. An emulsion formed. The solutions were equilibrated for 2 h. Then 5 ml of transparent supernatant was transferred to a different container, dried under a heat lamp for 4 h, and weighed. The calculated mass of SDS, present in the solutions, was subtracted from the observed mass to obtain the mass of DEP in the SDS solution.

APPENDIX B: BOUNDARY CONDITION ON THE SURFACE

The SDS concentration profile around a single DEP droplet dissolving in an aqueous SDS solution where the SDS concentration is below the critical micelle concentration is given by the general solution to the diffusion equation for a spherically symmetric profile

$$c(r) = C_1 - \frac{C_2}{r}, \quad (\text{B1})$$

where C_1 and C_2 are integration constants. It follows from the limit $r \rightarrow \infty$ that $C_1 = c_\infty$ is the bulk SDS concentration and C_2 is that at the droplet surface. To find this boundary condition, we use that the oil flux over the droplet surface j_{react} (in units of molecules $\text{m}^{-2} \text{s}^{-1}$) equals the diffusive flux of oil j_{diff} in the form of swollen micelles away from the surface. So for the oil transport,

$$j_{\text{react}} = k(c(a) - c^*) \frac{N_o}{N_s}, \quad (\text{B2})$$

$$j_{\text{diff}} = -N_s D_m \left. \frac{\partial c_m}{\partial r} \right|_{r=a}. \quad (\text{B3})$$

The value k is a velocity at which oil molecules move through the oil water interface and sets the rate of swollen micelle assembly, N_o is the number of oil molecules and N_s the number of surfactant molecules in a swollen micelle, D_m is the diffusion constant of swollen micelles, c_m is the

swollen micelle concentration, and a is the droplet radius. For steady-state surfactant transport, the diffusive transport of surfactant monomers toward the droplet $j_{\text{diff,in}}$ equals the outward surfactant flux in the form of oily micelles $j_{\text{diff,out}}$:

$$j_{\text{diff,out}} = -N_s D_m \left. \frac{\partial c_m}{\partial r} \right|_{r=a}, \quad (\text{B4})$$

$$j_{\text{diff,in}} = -D \left. \frac{\partial c}{\partial r} \right|_{r=a}. \quad (\text{B5})$$

Here D is the diffusion coefficient of SDS monomers. Combining these equations we find the following boundary condition for SDS at the droplet surface:

$$k(c(a) - c^*) = -D \left. \frac{\partial c}{\partial r} \right|_{r=a}. \quad (\text{B6})$$

This equation corresponds to the general boundary condition $c(a) + l \left. \frac{\partial c}{\partial r} \right|_{r=a} = \text{constant}$. Here $l \equiv D/k$. We compare Eq. (B1) with Eq. (B6) to find the value for the integration constant $C_2 = -\frac{a(c_\infty - c^*)}{1 + \frac{l}{a}}$, so that the concentration profile of SDS around a single diffusion drop is given by

$$c(r) = c_\infty - \frac{(c_\infty - c^*) a}{1 + \frac{l}{a}} \frac{1}{r}. \quad (\text{B7})$$

We now consider the two limiting cases: a constant surface concentration ($\frac{l}{a} \gg 1$), equivalent to a constant surface charge in electrostatics, and a constant surface expulsion ($\frac{l}{a} \ll 1$), equivalent to a constant potential in electrostatics. The regime of constant surface concentration corresponds to a diffusion-limited surface process. In this case the formation rate of oily micelles is much faster than the diffusion of SDS monomers to the surface and the concentration at the surface will equal the critical SDS concentration below which no assembly occurs. All SDS monomers beyond that concentration are instantly absorbed into swollen micelles. The concentration profile in this regime simplifies to

$$c(r) = c_\infty - (c_\infty - c^*) \frac{a}{r}. \quad (\text{B8})$$

In that regime, the surface concentration $c(a) = c^*$ and the dissolution rate $A = -D \left. \frac{\partial c}{\partial r} \right|_{r=a}$. Note that if the surface concentration is truly constant, no self-propulsion can occur, as there can be no variation in the surface concentration, so no surface gradient to induce motion. However, there will always be small variations in surface concentration to allow for swimming, albeit more slowly than one would expect in the regime of constant surface dissolution. Note that in the case of dissolving DEP droplets, the surface dissolution is negative because surfactant molecules are absorbed at the surface rather than expelled. Alternatively, the surface process can be reaction limited, so the assembly of swollen micelles at the surface is slower than the diffusive flux of monomers. Here the concentration profile is given by

$$c(r) = c_\infty - \frac{(c_\infty - c^*) a^2}{l} \frac{1}{r}. \quad (\text{B9})$$

Then surface concentration simplifies to $c(a) = c_\infty - \frac{a}{l}(c_\infty - c^*)$ and the dissolution rate simplifies to $A \equiv -D \left. \frac{\partial c}{\partial r} \right|_{r=a} = -k(c_\infty - c^*)$. In an exclusively rate-limited regime, no self-propulsion can occur either, as the reaction is very slow

and surface concentration becomes equal to the bulk SDS concentration. For a solute gradient along the particle surface to occur, the process should be predominantly one or the other.

APPENDIX C: ACTIVE PARTICLE IN AN EXTERNAL GRADIENT

The SDS consumption of one droplet modifies the external SDS gradient of a neighboring droplet ∇c_e to yield a gradient along the surface of that particle ∇c_s . We consider a single dissolving DEP droplet in a linear external SDS gradient G_{ext} with an angle-dependent SDS concentration $c(r, \theta)$. The steady-state diffusion profile is such that

$$\frac{1}{r^2} \frac{\partial c}{\partial r} \left(r^2 \frac{\partial c}{\partial r} \right) + \frac{1}{r^2 \sin(\theta)} \frac{\partial}{\partial r} \left[\sin(\theta) \frac{\partial c(r, \theta)}{\partial \theta} \right] = 0. \quad (\text{C1})$$

We next expand $c(r, \theta)$ in Legendre polynomials $P_n(\theta)$ to decouple the angular and radial components of the concentration gradient,

$$c(r, \theta) = \sum_{n=0}^{\infty} c_n(r) P_n(\theta) = c_0(r) + \cos(\theta) c_1(r) + \dots \quad (\text{C2})$$

We neglect all higher-order terms and use Eq. (C2) in the diffusion Eq. (C1). Because $\frac{\partial c(r, \theta)}{\partial r} = 0$, we find

$$c(r, \theta) = C_1 - \frac{C_2}{r} + \cos(\theta) \left(C_3 r + \frac{C_4}{r^2} \right), \quad (\text{C3})$$

where C_1 , C_2 , C_3 , and C_4 are all representing integration constants. To find C_1 and C_3 we consider the limit of $r \rightarrow \infty$. We applied a linear gradient with shape $G_{\text{ext}} x$ on top of a background concentration c_∞ so that the external concentration profile in polar coordinates is $c_{\text{lin}}(r, \theta) = G_{\text{ext}} r \cos(\theta) + c_\infty$ and we find $C_1 = c_\infty$ and $C_3 = G_{\text{ext}}$. Near the droplet, the flux over the droplet surface and the diffusive flux away from the droplet have to be equal, leading to a boundary condition similar to that in the previous section:

$$k[c(a, \theta) - c^*] = D \left. \frac{\partial c(r, \theta)}{\partial r} \right|_{r=a}. \quad (\text{C4})$$

Combining Eqs. (C3) and (C4) gives

$$\begin{aligned} c_\infty - c^* + \frac{C_2}{a} + \cos(\theta) \left(G_{\text{ext}} a + \frac{C_4}{a^2} \right) \\ = l \left[-\frac{C_2}{a^2} + \cos(\theta) \left(G_{\text{ext}} - \frac{2C_4}{a^3} \right) \right]. \end{aligned} \quad (\text{C5})$$

This has to be true for all values of θ so we find $C_2 = -\frac{a(c_\infty - c^*)}{1+l/a}$ and $C_4 = -a^3 G_{\text{ext}} \frac{1-l/a}{1+2l/a}$. The concentration profile $c(r, \theta)$ of a dissolving droplet in an external gradient of SDS is then Eq. (4) and the solute gradient along the particle surface ∇c_s is given by

$$\nabla c_s = \frac{c_1(a)}{a} = \frac{\frac{3l}{a}}{1 + \frac{2l}{a}} G_{\text{ext}}. \quad (\text{C6})$$

-
- [1] W. Wang, W. Duan, A. Sen, and T. E. Mallouk, *Proc. Natl. Acad. Sci. USA* **110**, 17744 (2013).
- [2] R. Soto and R. Golestanian, *Phys. Rev. Lett.* **112**, 068301 (2014).
- [3] A. Reinmüller, H. J. Schöpe, and T. Palberg, *Langmuir* **29**, 1738 (2013).
- [4] N. Kravchenko-Balasha, Y. S. Shin, A. Sutherland, R. D. Levine, and J. R. Heath, *Proc. Natl. Acad. Sci. USA* **113**, 5520 (2016).
- [5] N. Kravchenko-Balasha, J. Wang, F. Remacle, R. D. Levine, and J. R. Heath, *Proc. Natl. Acad. Sci. USA* **111**, 6521 (2014).
- [6] B. Abcassis, C. Cottin-Bizzone, C. Ybert, A. Ajdari, and L. Bocquet, *Nat. Mater.* **7**, 785 (2008).
- [7] N. J. Cira, A. Benusiglio, and M. Prakash, *Nature (London)* **519**, 446 (2015).
- [8] T. Toyota, N. Maru, M. M. Hanczyc, T. Ikegami, and T. Sugawara, *J. Am. Chem. Soc.* **131**, 5012 (2009).
- [9] M. D. Levan, *J. Colloid Interface Sci.* **83**, 11 (1981).
- [10] J. Elgeti, R. G. Winkler, and G. Gompper, *Rep. Prog. Phys.* **78**, 56601 (2015).
- [11] N. L. Abbott and O. D. Velev, *Curr. Opin. Colloid Interface Sci.* **21**, 1 (2016).
- [12] W. F. Paxton, S. Sundarajan, T. E. Mallouk, and A. Sen, *Angew. Chem., Int. Ed.* **45**, 5420 (2016).
- [13] S. Sengupta, M. E. Ibele, and A. Sen, *Angew. Chem., Int. Ed.* **51**, 8434 (2012).
- [14] J. Palacci, S. Sacanna, A. P. Steinberg, D. J. Pine, and P. M. Chaikin, *Science* **339**, 936 (2013).
- [15] S. Thutupalli, R. Seemann, and S. Herminghaus, *New J. Phys.* **13**, 073021 (2011).
- [16] I. Buttinoni, J. Bialké, F. K. Kömmel, H. Löwen, C. Bechinger, and T. Speck, *Phys. Rev. Lett.* **110**, 238301 (2013).
- [17] T. Sanchez, D. T. N. Chen, S. J. DeCamp, M. Heymann, and Z. Dogic, *Nature (London)* **491**, 431 (2012).
- [18] I. Theurkauff, C. Cottin-Bizonne, J. Pallaci, C. Yert, and L. Bocquet, *Phys. Rev. Lett.* **108**, 268303 (2012).
- [19] A. Brown and W. Poon, *Soft Matter* **10**, 4016 (2014).
- [20] S. Yabunaka and N. Yoshinaga, *J. Fluid Mech.* **806**, 205 (2016).
- [21] A. Banerjee, I. Williams, R. N. Azevedo, M. E. Helgeson, and T. M. Squires, *Proc. Natl. Acad. Sci. USA* **113**, 8612 (2016).
- [22] G. Faour, M. Grimaldi, J. Richou, and A. Bois, *J. Colloid Interface Sci.* **181**, 385 (1996).
- [23] N. Young, J. Goldstein, and M. Block, *J. Fluid Mech.* **3**, 6 (1959).
- [24] A. I. Fedosov (translated by B. Berenkov and K. Morozov), *Zh. Fiz. Khim.* **30**, 2 (1956).
- [25] Z. Izri, M. N. van der Linden, S. Michelin, and O. Dauchot, *Phys. Rev. Lett.* **113**, 248302 (2014).
- [26] S. Michelin, E. Lauga, and D. Bartolo, *Phys. Fluids* **25**, 1 (2013).
- [27] S. Yabunaka, T. Ohta, and N. Yoshinaga, *J. Chem. Phys.* **136**, 074904 (2012).
- [28] See Supplemental Material at <http://link.aps.org/supplemental/10.1103/PhysRevE.96.032607> for movies of the active interactions.
- [29] J. C. Crocker and D. G. Grier, *Phys. Rev. Lett.* **73**, 352 (1994).
- [30] B. J. Krishnatreya, A. Colen-Landy, P. Hasebe, B. A. Bell, J. R. Jones, A. Sunda-Meya, and D. G. Grier, *Am. J. Phys.* **82**, 23 (2014).
- [31] J. Clifford and B. A. Pethica, *J. Phys. Chem.* **70**, 3345 (1966).
- [32] M. F. Haase and J. Brujic, *Angew. Chem.* **53**, 11793 (2014).
- [33] T. H. Besseling, J. Jose, and A. van Blaaderen, *J. Microsc.* **257**, 142 (2015).